Dispersion of nonlinearity in subwavelength waveguides: derivation of pulse propagation equation and frequency conversion effects

Xuesong Zhao, Andrey V. Gorbach,* and Dmitry V. Skryabin

Centre for Photonics and Photonic Materials, Department of Physics, University of Bath, Bath BA2 7AY, UK
**Corresponding author: A.Gorbach@bath.ac.uk*

Received November 27, 2012; revised January 29, 2013; accepted February 4, 2013;
posted February 5, 2013 (Doc. ID 180685); published March 6, 2013

Description of pulse propagation in waveguides with subwavelength features and high refractive index contrasts requires an accurate account of the dispersion of nonlinearity due to the considerable mode profile variation with the wavelength. The corresponding model derived from asymptotic expansion of Maxwell equations contains a complicated network of interactions between different harmonics of the pulse, and therefore is not convenient for analysis. We demonstrate that this model can be reduced to the generalized nonlinear Schrödinger-type pulse propagation equation under the assumption of factorization of the four-frequency dependence of nonlinear coefficients. We analyze two different semiconductor waveguide geometries and find that the factorization works reasonably well within large wavelength windows. This allows us to utilize the pulse propagation equation for the description of a broadband signal evolution. We study the mechanism of modulational instability induced by the dispersion of nonlinearity and find that the power threshold predicted by the simple model with three interacting harmonics is effectively removed when using pulses, while the efficiency of this process grows for shorter pulse durations. Also, we identify the effects of geometrical and material dispersion of nonlinearity on spectral broadening of short pulses in semiconductor waveguides.

OCIS codes: 190.4390, 190.4223, 190.4410, 130.4310, 130.2790.

1. INTRODUCTION

With the recent remarkable progress in nanofabrication techniques, light propagation in subwavelength structures has attracted much attention. Semiconductor waveguides, such as silicon-on-insulator (SOI) [1,2] or AlGaAs [3], represent one of the promising platforms for light manipulation at the miniature scale. High refractive index contrast allows tight light confinement with typical waveguide transverse dimensions of the order of hundreds of nanometers (hence they are often referred to as photonic nanowires), while typical propagation losses are of the order of a few dB/mm [1].

Theoretical description of pulse propagation in conventional waveguides and fibers is largerly based on the well-established generalized nonlinear Schrödinger (NLS) model [4], which describes evolution of the guided mode envelope with propagation distance. The key strength of this model is in its simplicity. It contains two important ingredients: the group velocity dispersion (GVD) of the mode (responsible, e.g., for pulse spreading in time) and nonlinear interaction (resulting from light intensity-dependent refractive index of the medium). It is the interplay between these two ingredients that creates the plethora of effects in optical waveguides and fibers [4].

The NLS model is based on several approximations, among which is the assumption of a relatively small longitudinal electric field component of the mode (weak guidance) [4]. However, this is only true for waveguides with a relatively low refractive index contrast between the core and the cladding, and with core sizes being much larger than the wavelength of light. Development of adequate models to describe light propagation in subwavelength waveguides has become the subject of active research in the recent years [1,5–11].

One of the distinctive features of these waveguides is a strong variation of the modal profile with the wavelength of light. Since distribution of light intensity across the waveguide structure defines the effectiveness of nonlinear (multiphoton) processes, this variation leads to a considerable dispersion of nonlinearity [10,11]. Within the framework of the NLS model, it manifests through the appreciable dependence of the nonlinear waveguide parameter γ on frequency. The first-order dispersion of nonlinearity ($\gamma_1 = d\gamma/d\omega$) gives intensity-dependent correction to the group velocity. Such term appears in the pulse propagation equation even if an ideal homogeneous medium is considered, it is responsible for the self-steepening of pulses [4]. In subwavelength waveguides, the self-steepening effect can be significantly enhanced due to the geometrical contribution to the dispersion of nonlinearity [5,8,12]. Most important, the geometry-induced dispersion of nonlinearity can lead to a range of new effects. Recently we identified the novel mechanism of modulational instability (MI) of a constant-amplitude wave, mediated by the dispersion of nonlinearity in subwavelength waveguides [13]. We also introduced a simple phenomenological model describing this effect, which is based on the generalized version of the NLS equation where the second-order dispersion of nonlinearity term was added ($\gamma_2 = d^2\gamma/d\omega^2$). Similar models have been considered recently in the context of ultrashort pulse dynamics in fibers [14,15], beam propagation in nonlinear photonic crystals [16], pulse dynamics in

nonlinear metamaterials [17], and dynamics of Bose–Einstein condensate of dipolar atoms in a periodic potential [18].

It must be noted, that for the Kerr-type nonlinear response of a medium (the most common in optics), the nonlinear interaction involves four photons at different frequencies (four-wave mixing process). It is therefore the dependence on four frequencies of all the interacting waves, rather than single frequency dependence $\gamma(\omega)$ as in the above NLS models, which needs to be taken into consideration [1,7,8,13]. This can be done most naturally by considering pulse propagation in the frequency domain. However, the resulting model that describes evolution of individual harmonics with the propagation distance, the harmonic propagation (HP) model, contains a network of nonlocal nonlinear interactions [8,13], and appears to be complicated for analysis and resource demanding for numerical integration.

In this work, we demonstrate that the HP model, which is derived from Maxwell equations following the standard perturbation expansion procedure [1,5,7], can be reduced to the pulse propagation equation of NLS type with the dispersion of nonlinearity operator introduced—the nonlinear dispersive Schrödinger (NLDS) equation. The only assumption which allows this reduction is the factorization of the four-frequency dependence of nonlinear coefficients in HP model. Having analyzed different semiconductor subwavelength waveguide geometries, we found that this factorization approximates well the actual four-frequency dependencies in a wide range of wavelengths. This allows us to use the derived NLDS equation for the description of short pulse dynamics and parametric frequency conversion processes in subwavelength waveguides. Unlike the method proposed in [8], our approach does not require performing computationally heavy procedure of Taylor expansion of the modal profile frequency dependence, and is not limited by the narrow spectral width (quasi-CW) approximation.

2. PERTURBATION EXPANSION OF MAXWELL EQUATIONS AND HARMONIC PROPAGATION MODEL

We consider a waveguide defined by the linear dielectric permittivity ϵ and nonlinear Kerr susceptibility $\chi^{(3)}$. Both are functions of transverse coordinates (x, y), while the structure is homogeneous along the propagation direction z (see Fig. 1). We use Fourier expansion for the total electric field

$$\vec{\mathcal{E}}(\vec{\mathrm{r}},\mathrm{t}) = \frac{1}{\sqrt{2\pi}}\int \mathbf{E}(\vec{\mathrm{r}},\omega)\mathrm{e}^{-\mathrm{i}\omega\mathrm{t}}\mathrm{d}\omega + \mathrm{c.c.}, \tag{1}$$

where each harmonic is described in terms of slowly varying amplitude $A_\omega(z)$ of the corresponding linear mode:

$$\mathbf{E}(\vec{r},\omega) = I_\omega^{-1/2} A_\omega(z)\mathbf{e}_\omega(x,y), \tag{2}$$

$$I_\omega = \iint_{-\infty}^{+\infty} (\mathbf{e}_\omega \times \mathbf{h}_\omega^* + \mathbf{e}_\omega^* \times \mathbf{h}_\omega)\hat{e}_z \mathrm{d}x\mathrm{d}y. \tag{3}$$

Here $\hat{e}_z$ is the unit vector along z, $\mathbf{e}_\omega(x,y)$ and $\mathbf{h}_\omega(x,y)$ are the electric and magnetic field profiles of the linear mode at the frequency ω. The normalization is such that the power carried by each harmonic is given by $P_\omega = |A_\omega|^2$.

Displacement vector is assumed to have the form:

$$\mathbf{D}(\omega) = \epsilon_0[\epsilon(\omega)\mathbf{E}(\omega) + \chi^{(3)}(-\omega;\omega_1,-\omega_2,\omega_3)\vdots\mathbf{E}(\omega_1)\mathbf{E}^*(\omega_2)\mathbf{E}(\omega_3)], \tag{4}$$

where the third-order susceptibility tensor is given by $\chi^{(3)}_{iprs}(-\omega;\omega_1,-\omega_2,\omega_3) = \chi_{\omega\omega_2\omega_2\omega_3}[\rho(\delta_{ip}\delta_{rs}+\delta_{ir}\delta_{ps}+\delta_{is}\delta_{pr})/3 + (1-\rho)\delta_{iprs}]$ [1,7]. δ_{ij} is the Kronecker delta and ρ is the nonlinear anisotropy parameter ($\rho = 1$ in the isotropic approximation). For silicon $\rho \approx 1.27$ [7]; for all other materials in Fig. 1, we took $\rho = 1$.

Following a similar procedure as described in [1,7], we derive equations for the harmonic amplitudes (HP model):

$$i\partial_z A_\omega = -\beta_\omega A_\omega - \frac{\omega}{2\pi}\iint \Gamma_{\omega\omega_1\omega_2\omega_3} A_{\omega_1} A^*_{\omega_2} A_{\omega_3} \mathrm{d}\omega_1 \mathrm{d}\omega_2, \tag{5}$$

$$\omega_3 = \omega - \omega_1 + \omega_2, \tag{6}$$

where β_ω is the propagation constant of the linear-guided mode at the corresponding frequency, and nonlinear coefficients are given by

$$\Gamma_{nklm} = \frac{\epsilon_0}{\sqrt{I_n I_k I_l I_m}}\iint_{-\infty}^{+\infty} \chi_{nklm}\zeta_{nklm}\mathrm{d}x\mathrm{d}y, \tag{7}$$

$$\zeta_{nklm} = \rho[(\mathbf{e}_n^*\mathbf{e}_m)(\mathbf{e}_k\mathbf{e}_l^*) + (\mathbf{e}_n^*\mathbf{e}_k)(\mathbf{e}_m\mathbf{e}_l^*) + (\mathbf{e}_n^*\mathbf{e}_l^*)(\mathbf{e}_k\mathbf{e}_m)] + 3(1-\rho)\sum_{i=x,y,z} e_{ni}^* e_{ki} e_{li}^* e_{mi}. \tag{8}$$

Material dispersion of nonlinearity is usually weak and also poorly characterized in terms of its variations with multiple frequencies. It is thus practical to assume

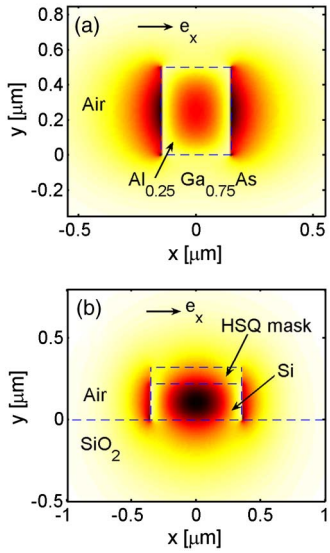

Fig. 1. (Color online) Geometry and profile of the dominant electric field component (e_x) of the quasi-TE guided mode in subwavelength semiconductor waveguides: (a) AlGaAs waveguide, $\lambda_0 = 1.665$ μm and (b) SOI waveguide, $\lambda_0 = 2.3$ μm.

$\chi_{nklm} \equiv \chi = (4/3)\epsilon_0 \epsilon c n_2$, where the Kerr coefficient n_2 and dielectric permittivity ϵ are evaluated at a reference frequency $\omega_0 = 2\pi c/\lambda_0$. Contrary, geometrical dispersion of nonlinearity is expected to be strong in subwavelength waveguides [10,11], and its role is elucidated below.

3. FACTORIZATION OF NONLINEAR COEFFICIENTS AND PULSE PROPAGATION EQUATION

The geometrical dispersion is accounted for by the coefficients ζ_{nklm} in Eq. (8). Definition of these coefficients involves overlap integrals with modal profiles at different frequencies. We note that ζ_{nklm} are invariant under all permutations of indices that preserve the condition $n-k+l-m=0$: $\zeta_{nklm} = \zeta_{lknm} = \zeta_{nmlk} = \zeta_{mlkn} = \zeta_{knml} = \zeta_{mnkl}$.

Even with the account of the above symmetry, description of a broadband signal evolution within the HP model in Eq. (5) remains to be a challenging computational task due to the large number of nonlinear coefficients to be computed. In the view of the above permutation symmetry, a significant reduction can be made by assuming factorization of nonlinear coefficients:

$$\Gamma_{nklm} \approx g_n g_k g_l g_m, \qquad g_n = \Gamma_{nnnn}^{1/4} \equiv \Gamma_n^{1/4}. \tag{9}$$

We test this approximation by direct comparison with the original coefficients obtained from Eq. (7). In Fig. 2 the relative error $\Delta = |\Gamma_{nklm} - g_n g_k g_l g_m|/\Gamma_n$ is plotted in the plane of parameters $\delta_{k,l} = (\omega_{k,l} - \omega_n)/\omega_n$ for the fixed $\omega_n \approx 1.13 \cdot 10^{15}$ rad/s ($\lambda_n = 2\pi c/\omega_n = 1.665$ μm) and the AlGaAs waveguide geometry as in Fig. 1(a). Remember, the fourth frequency ω_m is determined by the resonance condition in Eq. (6). Apparently, the error remains to be small, $\Delta < 10^{-1}$, within a large window of frequency detunings ($\delta_{k,l} = 0.25$ corresponds to $\delta\lambda \approx 0.5$ μm). We obtained similar results for other fixed values of ω_n, as well as for the silicon waveguide geometry as in Fig. 1(b). Note that certain one-dimensional subsets of coefficients with $\delta_k = \delta_l$, $\delta_k = 0$, $\delta_l = 0$ enter the condition of MI of the constant amplitude pump at the frequency ω_n, as discussed in the next section. Further comparison between the corresponding factorized and full coefficients Γ is illustrated in Fig. 4.

Replacing coefficients Γ_{nklm} with their factorized analogs and changing to variables

$$A_n = (g_0/g_n)\Psi_n, \tag{10}$$

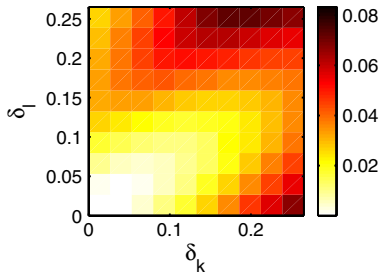

Fig. 2. (Color online) Relative factorization error Δ for the AlGaAs waveguide as in Fig. 1(a) and the fixed frequency $\omega_n = 2\pi c/\lambda_n$, $\lambda_n = 1.665$ μm; see text for details.

where $g_0 = \Gamma_0^{1/4}$ corresponds to a reference frequency ω_0. Equation (5) becomes:

$$i\partial_z \Psi_\omega = -\beta_\omega \Psi_\omega - \frac{\tilde{\gamma}_\omega}{2\pi} \iint \Psi_{\omega_1} \Psi^*_{\omega_2} \Psi_{\omega_3} \mathrm{d}\omega_1 \mathrm{d}\omega_2, \tag{11}$$

where we introduced the modified nonlinear coefficient:

$$\tilde{\gamma}_\omega = \omega \sqrt{\Gamma_0 \Gamma_\omega}. \tag{12}$$

It is possible to show that Eq. (11) possesses two integrals of motion [18]:

$$P = \int \frac{\omega |\Psi_\omega|^2}{\tilde{\gamma}_\omega} \mathrm{d}\omega = \text{const.}, \tag{13}$$

$$N = \int \frac{|\Psi_\omega|^2}{\tilde{\gamma}_\omega} \mathrm{d}\omega = \text{const.} \tag{14}$$

In terms of the original harmonic amplitudes A_n, these integrals correspond to the total power and the classical analog of the number of photons, respectively.

Assuming polynomial fits of the linear and nonlinear dispersion coefficients in Eq. (11): $\beta(\omega = \omega_0 + \delta) = \sum_{n=0}^{N_D} (1/n!)\beta_n \delta^n$, $\tilde{\gamma}(\omega = \omega_0 + \delta) = \sum_{n=0}^{N_G} (1/n!)\tilde{\gamma}_n \delta^n$, using inverse Fourier transform

$$\psi(z,t) = \frac{1}{\sqrt{2\pi}} \int \Psi_\omega(z) e^{-i(\omega_0+\delta)t} \mathrm{d}\delta, \tag{15}$$

and transforming into the rotating and moving frame $\psi(z,t) = a(\tau = t - \beta_1 z, z) e^{i\beta_0 z}$, we obtain the following pulse propagation (NLDS) equation:

$$i\partial_z a = -\hat{D}(i\partial_\tau)a - \hat{G}(i\partial_\tau)(|a|^2 a), \tag{16}$$

$$\hat{D}(i\partial_\tau) = \sum_{n=2}^{N_D} \frac{\beta_n}{n!} (i\partial_\tau)^n, \tag{17}$$

$$\hat{G}(i\partial_\tau) = \sum_{n=0}^{N_G} \frac{\tilde{\gamma}_n}{n!} (i\partial_\tau)^n. \tag{18}$$

We emphasize that the factorization of coefficients Γ_{nklm} in Eq. (9) is the only approximation made to derive the above NLDS equation form the HP model in Eq. (5). The dispersion of nonlinearity operator $\hat{G}$ in Eqs. (16) and (18) is linked to the modified nonlinear coefficient $\tilde{\gamma}(\omega)$, which is different from the conventional nonlinear coefficient $\gamma = \omega \Gamma_\omega$ [1,4,7], see Eq. (12) and Figs. 3 and 10(b). If a narrowband signal is considered, the polynomial expansion coefficients $\tilde{\gamma}_n$ can be replaced by the standard Taylor coefficients: $\tilde{\gamma}_n = d^n \tilde{\gamma}/d\omega^n$. One can relate these coefficients to the corresponding Taylor expansion coefficients of the function γ, $\gamma_n = d^n \gamma/d\omega^n \equiv d^n(\omega\Gamma_\omega)/d\omega^n$. For the first three coefficients we obtain:

$$\tilde{\gamma}_0 = \gamma_0, \tag{19}$$

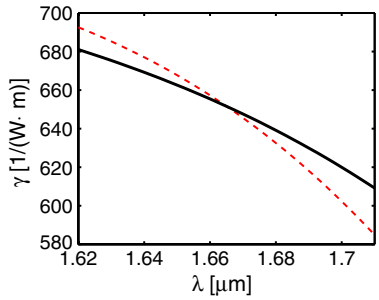

Fig. 3. (Color online) Modified nonlinear coefficient $\tilde{\gamma}$ for AlGaAs waveguide; see Eq. (12). Dashed curve shows the conventional nonlinear coefficient $\gamma = \omega\Gamma_\omega$ for the same waveguide.

$$\tilde{\gamma}_1 = \frac{1}{2}\left(\frac{\gamma_0}{\omega_0} + \gamma_1\right), \tag{20}$$

$$\tilde{\gamma}_2 = \frac{\gamma_2}{2} - \frac{(\gamma_1 - \gamma_0/\omega_0)^2}{4\gamma_0}. \tag{21}$$

When geometrical dispersion of nonlinearity is absent ($\Gamma = \text{const.}$), $\tilde{\gamma}_{i>1} = 0$ and the first-order dispersion coefficient is reduced to the standard self-steepening term [4]: $\tilde{\gamma}_1 = \gamma_0/\omega_0$.

Below, we exploit the pulse propagation Eq. (16) to analyze the role of dispersion of nonlinearity in ultrashort pulse dynamics and parametric frequency conversion. In our modeling, we computed coefficients Γ_ω (7) from modal profiles which, together with the corresponding propagation constants β_ω, were obtained with the help of a commercially available Maxwell solver package. NLDS Eq. (16) was then numerically integrated by the standard split-step procedure [4], where the nonlinear step was computed in frequency domain by the fourth-order Runge–Kutta method. Finally, the output field was converted to the modal amplitudes A by applying the scaling in frequency domain, see Eq. (10).

4. MODULATIONAL INSTABILITY AND FREQUENCY COMB GENERATION

MI is a well-known nonlinear process where a constant amplitude pump wave at a frequency ω_p creates parametric gain for the sidebands at frequencies ω_s (signal) and $\omega_i = 2\omega_p - \omega_s$ (idler). The onset of MI can be analyzed and numerically modeled with the help of the reduced HP model, which includes only three interacting harmonics [13]. However, its evolution generally leads to generation of multiple higher-order harmonics, see Fig. 8(a). To model such process, the NLDS Eq. (16) appears to be more convenient. Moreover, it allows one to identify specific features of MI process when dealing with pulsed excitation. Below, we compare the two models by considering three interacting harmonics, and then proceed with numerical analysis of MI evolution with pulses by using the NLDS model.

Reducing Eq. (5) to the case of three interacting waves, and considering weak amplitudes of the signal and idler, we obtain:

$$i\partial_z A_p = -\beta_p A_p - \omega_p \Gamma_p |A_p|^2 A_p, \tag{22}$$

$$i\partial_z A_s = -\beta_s A_s - 2\omega_s \Gamma_{sp} |A_p|^2 A_s - \omega_s \Gamma_4 A_p^2 A_i^*, \tag{23}$$

$$i\partial_z A_i = -\beta_i A_i - 2\omega_i \Gamma_{ip} |A_p|^2 A_i - \omega_i \Gamma_4 A_p^2 A_s^*. \tag{24}$$

For convenience we use short subscripts p, s, i instead of ω_p, ω_s, ω_i, $\Gamma_p \equiv \Gamma_{pppp}$, $\Gamma_{sp} \equiv \Gamma_{spps}$, $\Gamma_{ip} \equiv \Gamma_{ippi}$, $\Gamma_4 \equiv \Gamma_{spip} = \Gamma_{ipsp}$. Assuming A_s, $A_i \sim e^{\kappa z}$, parametric amplification occurs when $g = \mathrm{Re}(\kappa) > 0$. From Eqs. (22)–(24) it is straightforward to derive the corresponding condition of existence of MI [13]:

$$4\gamma_- |A_p|^2 < \delta\beta < 4\gamma_+ |A_p|^2, \tag{25}$$

$$\gamma_\pm = \left(\omega_s \Gamma_{sp} + \omega_i \Gamma_{ip} - \omega_p \Gamma_p \pm \sqrt{\omega_s \omega_i} \Gamma_4\right)/2, \tag{26}$$

where $\beta_{p,s,i} = \beta(\omega_{p,s,i})$.

Neglecting dispersion of nonlinearity, i.e., assuming all coefficients Γ in Eq. (26) to be equal, it is easy to see that $\gamma_- > 0$, and therefore MI is only possible when $\delta\beta > 0$, which is the well-known textbook condition [4]. In particular, if $\beta(\omega)$ can be approximated by a parabola in a vicinity of ω_p [i.e., $\beta_{i>2} = 0$ in Eq. (17)], this condition is reduced to $\beta_2 = \partial_\omega^2 \beta(\omega_p) < 0$, which corresponds to anomalous GVD, see Fig. 5(a).

Dispersion of nonlinearity is responsible for the novel mechanism of MI that can be observed with $\delta\beta < 0$ (*normal* GVD), provided $\gamma_- < 0$ [13]. Note that a frequency-dependant Γ is needed to enable negative γ_-, which generally implies $\tilde{\gamma}_2 = \partial_\omega^2 \tilde{\gamma} \neq 0$, see Eq. (12).

Different coefficients Γ entering the condition in Eq. (25) are plotted for the AlGaAs and silicon waveguides in Figs. 4(a) and 4(b), respectively. Apparently, in both examples, factorization approximation works well in a wide range of signal/idler wavelengths, and therefore one can benefit from using the more convenient for analysis pulse propagation equation (16).

Neglecting higher than second-order dispersions of nonlinearity in the NLDS Eq. (16), $\gamma_-(\delta \equiv \omega_p - \omega_s)$ is given by:

$$2\gamma_- = \tilde{\gamma}_0 + \tilde{\gamma}_2 \delta^2 - \sqrt{\left(\tilde{\gamma}_0^2 + \frac{\tilde{\gamma}_2}{2}\delta^2\right)^2 - \tilde{\gamma}_1^2 \delta^2}. \tag{27}$$

From this expression, we derive that γ_- is always negative for small enough detunings δ, provided the following condition is satisfied:

$$G = \frac{\tilde{\gamma}_0 \tilde{\gamma}_2}{\tilde{\gamma}_1^2} < -1. \tag{28}$$

For the typical case of focusing Kerr nonlinearity, the nonlinear coefficient is positive: $\tilde{\gamma}_0 > 0$, and therefore the above condition implies, in particular, that $\tilde{\gamma}_2 < 0$. While only one coefficient Γ_ω is needed to compute the modified nonlinear coefficient $\tilde{\gamma}$, see Eq. (12), the condition in Eq. (28) is much more convenient for analysis of MI, as compared to the direct computation of γ_- from Eq. (26).

As an example, we consider a suspended 300 nm × 500 nm $Al_{0.25}Ga_{0.75}As$ waveguide [3,13] with the geometry and profile of one of the guided modes (dominant electric field component is oriented horizontally) shown in Fig. 1(a). The GVD of this mode is normal ($\beta_2 > 0$) for $\lambda > 1.66$ μm, see Fig. 5(a).

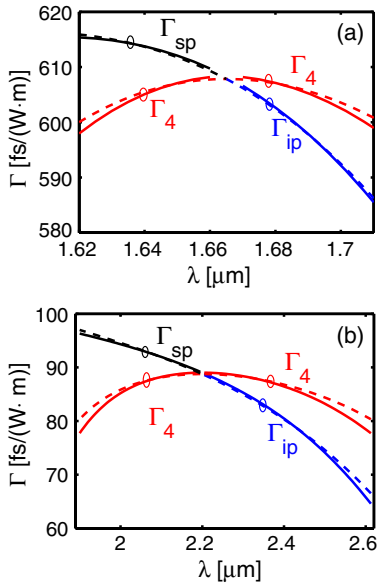

Fig. 4. (Color online) Dispersion of nonlinearity: nonlinear coefficients Γ entering the necessary condition for MI [see Eq. (26)] calculated for AlGaAs waveguide at (a) $\lambda_p = 1.65$ μm and (b) SOI waveguide at $\lambda_p = 2.2$ μm. Dashed curves show their factorized approximations, see Eq. (9).

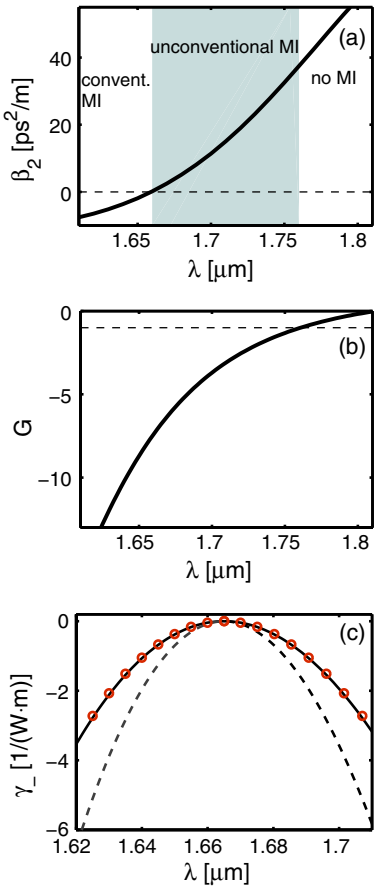

Fig. 5. (Color online) MI in AlGaAs waveguide: (a) group velocity dispersion, conventional MI is possible in the range of anomalous GVD, $\beta_2 < 0$. Shaded area indicates the region of unconventional MI due to the dispersion of nonlinearity. (b) Condition for $\gamma_- < 0$, see Eq. (28). (c) γ_- calculated for $\lambda_p = 1.665$ μm from Eq. (27) by using Taylor expansion coefficients of $\tilde{\gamma}(\omega)$, solid curve, and $\gamma(\omega)$, dashed curve. Red/gray circles correspond to γ_- calculated from Eq. (26).

The nonlinear coefficient $\tilde{\gamma}$ is shown in Fig. 3. Analysis of the condition in Eq. (28) indicates possibility to observe MI in a wide window of wavelengths within the range of normal GVD: 1.66 μm $< \lambda <$ 1.76 μm, see Fig. 5(b) and shaded area in Fig. 5(a). Choosing $\lambda_p = 2\pi c/\omega_p = 1.665$ μm, we compute γ_- by using the original definition in Eq. (26) and the reduced expression in Eq. (27); both appear to be in good agreement as shown in Fig. 5(c). For comparison, we also compute γ_- by using the standard definition of the nonlinear coefficient, i.e., by replacing all $\tilde{\gamma}_i$ with γ_i in Eq. (27), see the dashed curve in Fig. 5(c). Apparently, the modified nonlinear coefficient, which has been derived on the basis of the factorization approximation in Eq. (9), gives a much better agreement with the original model in Eq. (5).

The computed coefficient γ_- is negative in the broad range of the signal and idler wavelengths. This result is consistent with the condition in Eq. (28). While $\delta\beta$ is negative for the chosen pump wavelength, see Fig. 6(a), MI can be provided only through the mechanism related to the dispersion of nonlinearity. Figure 6(b) shows the computed gain coefficient g for the pump power of $|A_p|^2 = 150$ W. In this case, the maximum gain of $g \approx 5000$ m^{-1} is achieved for the signal located at around $\lambda_s = 1.7$ μm (idler is at $\lambda_i = 1.63$ μm), and the corresponding length of the development of MI is $L_{\mathrm{MI}} = 1/g \approx 0.2$ mm.

While the condition in Eq. (26) was obtained under approximation of three interacting harmonics, to analyze the role of finite pump bandwidth and higher harmonics excitation in the development of MI, we performed numerical simulations of NLDS Eq. (16) with the input field consisting of two 100 ps sech pulses: a high-power pump pulse centered at $\lambda_p =$ 1.665 μm (peak power 150 W) and a weak-power signal at $\lambda_s = 1.7$ μm (peak power 0.1 mW). The signal pulse triggers MI and is located at the wavelength for which the maximum gain is predicted when CW pump of the same power is used, see Fig. 6(b). Such setup corresponds to the case of seeded MI [19] and requires relatively short propagation distances if compared to noise- or waveguide impurity-induced MI. The orders of polynomial expansions of linear and nonlinear dispersion operators, Eqs. (17) and (18), were taken as $N_D = 11$ and $N_G = 7$, respectively, providing with a good fit of numerically computed functions $\beta(\omega)$ and $\tilde{\gamma}(\omega)$ across the range of wavelengths 1.4 μm $< \lambda <$ 2 μm.

A typical output spectrum after the propagation distance of $z = 0.4$ mm is shown in Fig. 7(a). Both signal and idler are boosted in power due to the development of MI. To confirm the importance of the dispersion of nonlinearity in this process, we repeated simulations with the truncated versions of the nonlinear operator in Eq. (18) having $N_G = 0$ (wavelength-independent nonlinearity) and $N_G = 1$ (self-steepening only). In both cases, the output signal and idler spectral peaks are similar (they are nonzero because the signal is seeded) and significantly lower than those with the full dispersion of nonlinearity operator, see Fig. 7(a).

In Fig. 7(b) the conversion efficiency $\eta = P_{i,\mathrm{out}}/P_{s,\mathrm{in}}$ [19] is plotted as function of the pump pulse peak power. The input signal power, $P_{s,\mathrm{in}}$, and output idler power, $P_{i,\mathrm{out}}$, were computed by the integration of the respective narrow frequency intervals. According to the analytical estimation based on the three waves approximation, no gain is possible below

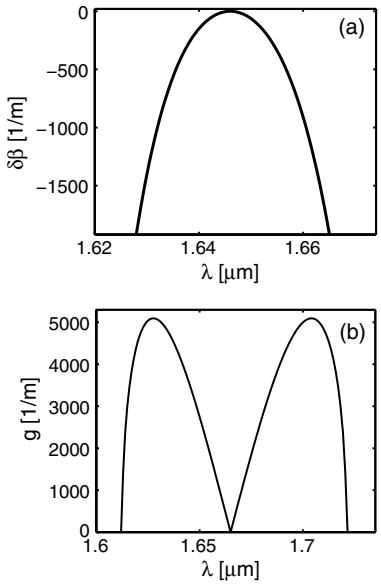

Fig. 6. Dispersion of nonlineriaty induced MI in AlGaAs waveguide: $\delta\beta$ (a) and calculated gain (b), for the pump wavelength $\lambda_p = 1.665$ μm and pump power $|A_p|^2 = 150$ W.

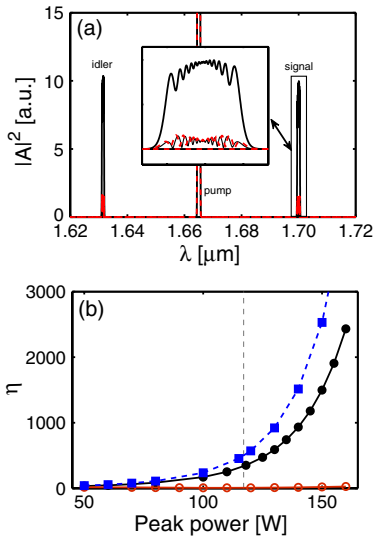

Fig. 7. (Color online) MI development with 100 ps pulse excitation: (a) output spectra after $z = 0.4$ mm propagation distance. Thin solid curve corresponds to wavelength-independent nonlinearity, dotted red/gray curve to self-steepening only, and thick solid curve to full dispersion of nonlinearity. Pump peak power is 150 W. (b) Conversion efficiency as a function of the pump peak power. Full/open circles correspond to the full/self-steepening only dispersion of nonlinearity. Full squares correspond to the same as full circles, but for 10 ps pulse excitation. Vertical dashed line indicates the threshold power for the case of three interacting waves [13]. The signal peak power is fixed to 0.1 mW in all simulations.

the threshold pump power $P_{\text{th}} = \delta\beta/\gamma_-$, while above this threshold the gain increases with pump power [13]. For the chosen signal wavelength, we estimate the threshold power to be $P_{\text{th}}(\lambda_s = 1.7\ \mu\text{m}) \approx 115$ W, see the vertical dashed line in Fig. 7(b). When using pulse excitation, we found that the conversion efficiency grows steadily with the pump power. Note that if we keep the self-steepening type of dispersion of nonlinearity only, the conversion efficiency remains low at all powers, see open circles in Fig. 7(b). This confirms that the observed gain is due to the higher-order dispersion of nonlinearity.

For shorter pulse durations we obtained qualitatively similar results, but the conversion efficiency becomes higher, see full squares in Fig. 7(b). This growth can be explained by the spectral broadening of the signal and idler due to the self-phase modulation [4], which becomes more pronounced for shorter pulses. The broadening effectively acts as a secondary seed, expanding the range of seed/idler frequencies to be parametrically amplified.

As the signal and idler are amplified, their interaction with the pump produces higher-order sidebands. The process is repeated in the cascaded manner, eventually leading to the generation of a frequency comb, see Fig. 8(a). In time domain, this corresponds to the formation of a periodic sequence of ultrashort pulses, see Fig. 8(b).

5. SPECTRAL BROADENING IN SOI WAVEGUIDE

In this section, we discuss the impact of dispersion of nonlinearity on spectral broadening of ultrashort pulses. This renowned phenomenon occurs in a wide range of nonlinear media. Particularly in optical fibers, octave-wide spectral broadening from a subpicosecond pulse, optical supercontinuum, has been studied for decades and applied to a range of fields as the convenient tool for generation of coherent radiation [20]. The theoretical foundation for spectral broadening in optical fibers is well established nowadays; in particular, it is recognized that the phenomenon occurs as the interplay between linear dispersion and nonlinearity. The broadest spectra are achieved by pumping near the zero GVD wavelength, where the dispersion changes its sign from anomalous to normal or vice versa [20].

Recently, spectral broadening and frequency conversion in SOI waveguides has become a focus of research [21,22]. High nonlinear coefficient of silicon, combined with strong and tunable dispersion of SOI nanowaveguides, ensures nonlinear effects happening more effectively and over much shorter propagation distances than in conventional fibers. However, silicon has strong two-photon absorption (TPA) near the standard telecom wavelength of $\lambda = 1.55$ μm [23], which brings major limitations to the nonlinear performance of SOI waveguides. TPA can be characterized by the ratio α_{TPA} of the real and imaginary parts of the nonlinear susceptibility of silicon [5]:

$$\chi^{(3)} = \chi(1 + i\alpha_{\text{TPA}}). \tag{29}$$

Figure 9 shows the experimental data for α_{TPA} in bulk silicon (adapted from [23]) together with a simple fit $\alpha_{\text{TPA}} = 0.03/\pi \cdot [\arctan((\omega - \omega_c)/w) + \pi/2]$, $\lambda_c = 2\pi c/\omega_c = 1.97\,\mu\text{m}$, $w = 2 \cdot 10^{13}$ s^{-1}, used in our calculations. As one can see, TPA sharply drops and becomes practically negligible beyond 2 μm.

We choose the geometry of SOI waveguide shown in Fig. 1(b). For the selected waveguide dimensions, the quasi-TE mode has zero GVD at $\lambda \approx 2.27$ μm, see Fig. 10(a). By pumping near this wavelength, one should expect to benefit from a reduced TPA rate. Figure 11 illustrates spectral broadening for the case of 100 fs input sech pulse with

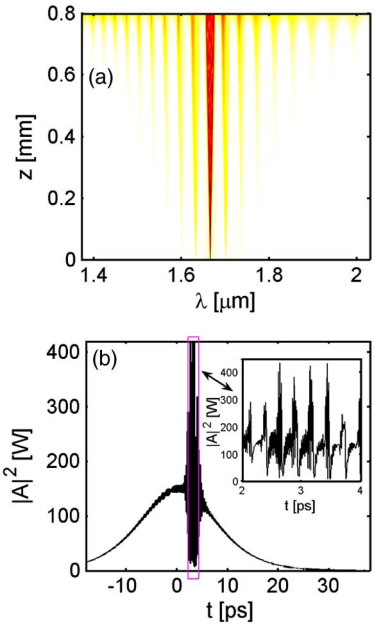

Fig. 8. (Color online) MI development with 10 ps pulse excitation: (a) evolution of the spectrum with propagation distance and (b) output signal in time domain after the propagation distance of $z = 0.8$ mm. The inset zooms in the central region of the pulse, where formation of a periodic sequence of ultrashort pulses is clearly visible. The pump/seed peak power is 150 W/0.1 mW; other parameters are the same as in Fig. 7.

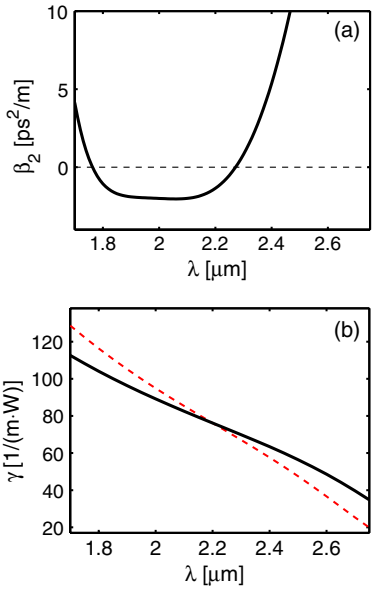

Fig. 10. (Color online) (a) Calculated GVD and (b) nonlinear coefficient (real part), for the quasi-TE mode of SOI waveguide shown in Fig. 1(b). Solid/dashed curve in (b) corresponds to the modified/conventional ($\tilde{\gamma}/\gamma$) nonlinear coefficient. In numerical simulations, we used polynomial fits of orders $N_D = 6$ and $N_G = 4$ to reproduce $\beta_2(\omega)$ and $\tilde{\gamma}(\omega)$ dependencies, respectively.

the peak power of 100 W and central wavelength of $\lambda_0 = 2.2$ μm. This result was obtained by numerical integration of Eq. (16) with the wavelength-independent nonlinear coefficient, i.e., $N_G = 0$ in the expansion of the nonlinear operator in Eq. (18), and with no account of TPA. The spectrum evolves following the typical two-stage scenario [20]. At the first stage ($0 < z < 0.7$ mm) spectrum broadens symmetrically due to the self-phase modulation of the pulse. For larger distances, the interplay between dispersion and nonlinearity becomes important. This causes a considerable spectral asymmetry, with more power being concentrated in the long-wavelength part of the spectrum.

After $z = 1$ mm propagation distance, the output spectrum covers the wide range of wavelengths 1.8 μm $< \lambda <$ 2.6 μm. According to our calculations, the real part of the nonlinear coefficient changes significantly in this wavelength range, see Fig. 10(b). Also, a large part of the output spectrum falls into the range of strong TPA. Therefore, both geometrical and material dispersions of nonlinearity are expected to influence the spectral broadening process.

In Fig. 12, output spectra are compared for three different cases: with constant nonlinear coefficient, self-steepening only, and full geometrical dispersion of nonlinearity. TPA was disregarded in all these simulations. Self-steepening enhances spectral asymmetry by lowering and shifting peak in the short-wavelength part of the spectrum and separating the long-wavelength edge spectral peak from the central three-peak structure formed during the self-phase modulation stage. Geometrical dispersion further boosts the asymmetry, especially enhancing features in the long-wavelength wing.

The effect of dispersion of TPA is summarized in Fig. 13, where we compare cases of no TPA, wavelength-independent TPA, and dispersive TPA. As expected, inclusion of flat TPA rate $\alpha_{\mathrm{TPA}} \equiv 0.03$ results in overall shrinking of the spectrum. Perhaps more surprisingly, fully dispersive TPA does not bring any noticeable spectral assymetries and effectively acts as a reduced flat TPA. The reason for that is in the link between short- and long-wavelength wings of the spectrum, which has

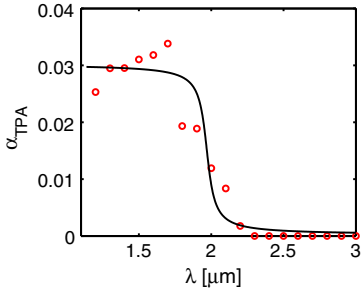

Fig. 9. (Color online) TPA rate in bulk silicon: experimental data adapted from [23] (circles) and analytical fit used in our calculations (solid curve).

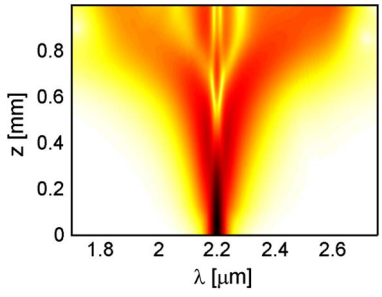

Fig. 11. (Color online) Spectral broadening in SOI waveguide pumped at $\lambda_0 = 2.2$ μm by a 100 fs pulse with 100 W peak power. The result is obtained for the case of wavelength-independent nonlinear coefficient, $\tilde{\gamma} = \mathrm{const}$. TPA is neglected.

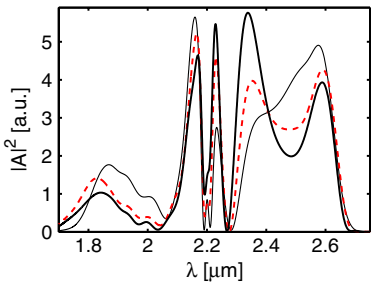

Fig. 12. (Color online) Spectral broadening in SOI waveguide: geometrical dispersion of nonlinearity. Output spectra at $z = 1$ mm calculated for the cases of wavelength-independent nonlinearity $\tilde{\gamma} = \text{Const}$. (thin solid curve), self-steepening nonlinearity $\tilde{\gamma} = \omega\Gamma_0$ (dashed red/gray curve), and fully dispersive nonlinearity $\tilde{\gamma} = \omega\sqrt{\Gamma_0\Gamma}$ (thick solid curve). Input parameters are the same as in Fig. 11.

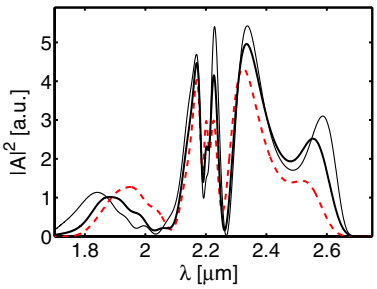

Fig. 13. (Color online) Spectral broadening in SOI waveguide: dispersion of TPA. Output spectra at $z = 1$ mm calculated for the cases of no TPA (thin solid curve), wavelength-independent TPA $\alpha_{\text{TPA}} \equiv 0.03$ (dashed red/gray curve), and dispersive TPA (thick solid curve) as in Fig. 9. Full geometrical dispersion of nonlinearity is taken into account. Input parameters are the same as in Fig. 11.

been analyzed in details in the context of supercontinuum generation in fibers [20]. In particular, spectral features in the normal GVD wing of generated supercontinua are generally defined by the positions and intensities of spectral peaks in the anomalous GVD wing. Apparently, this relation holds in the NLDS model: while TPA affects mostly the short-wavlength wing of the spectrum (where GVD is anomalous), the spectral peaks in the long-wavlength wing (normal GVD) change accordingly.

6. SUMMARY

The HP model in Eq. (5), derived from Maxwell equations following the perturbation expansion procedure, can be reduced to the NLDS pulse propagation Eq. (16) by introducing factorization of the four-frequency dependence of the nonlinear coefficients Γ_{nklm}. Although this procedure is not exact, it is supported by the symmetries of the coefficients Γ_{nklm} with respect to certain permutations of indices. The factorization was tested on different semiconductor waveguide geometries and found to approximate well the actual coefficients in wide wavelength ranges. Unlike previously derived models [1,5,7], the pulse propagation Eq. (16) takes full account of the dispersion of nonlinearity, is not limited by the quasi-CW approximation, and therefore can be applied for analysis of parametric frequency conversion effects.

We exploited the pulse propagation Eq. (16) to study the novel type of MI, induced by the dispersion of nonlinearity, in close to experimental conditions, where a high peak power pump pulse is initially perturbed by a weak signal pulse (seeded MI). Our results indicate that spectral broadening of pulses due to the self-phase modulation plays an important role in the development of MI. In particular, MI is observed for pump pulse peak powers well below the threshold predicted for CW pump [13]. In addition, the conversion efficiency becomes higher when shorter pulses are used. Similar to the conventional MI, long-term evolution of the dispersion of nonlinearity induced MI leads to the cascaded generation of higher-order sidebands and associated formation of a sequence of ultrashort pulses.

We also considered the impact of the dispersion of nonlinearity on spectral broadening of short pulses in a SOI waveguide. We chose the geometry where the zero of GVD is located at around $\lambda = 2.27$ μm. Pumping by 100 fs pulses with 100 W peak power in a vicinity of this wavelength, a considerable spectral broadening can be observed with output spectra spanning from 1.8 to 2.6 μm. The nonlinear coefficient changes significantly in this wavelength range, causing clearly pronounced spectral asymmetries. Also, for silicon, the ratio of TPA to Kerr coefficients changes sharply around $\lambda = 2.2$ μm, reaching its highest rate of $\alpha_{\text{TPA}} \approx 0.03$ below 1.9 μm and being practically zero above 2.1 μm. However, the account for dispersive imaginary part of the nonlinear coefficient does not introduce any noticeable additional asymmetry in the output spectra, causing nearly even shrinkage and power loss on either side of the spectrum. This counterintuitive result is explained by the internal link between the edges of the spectrum, well analyzed in the context of optical fibers [20]. Although the long-wavelength wing remains in the range of negligibly small TPA, its structure still changes accordingly with the short-wavelength wing, the latter being affected by the strong TPA.

The above examples illustrate the convenience of the NLDS model in Eq. (16) for analysis of nonlinear processes involving broadband signal evolution in waveguides, where dispersion of nonlinearity is considerable. The factorization approximation, which enables exertion of this model, can be tested directly for a particular geometry. A careful analysis of the general conditions of applicability of this approximation remains to be the challenging task for future research.

ACKNOWLEDGMENTS

The work was supported by the Engineering and Physical Sciences Research Council project EP/G044163/1.

REFERENCES

1. R. M. Osgood, Jr., N. C. Panoiu, J. I. Dadap, X. Liu, X. Chen, I.-W. Hsieh, E. Dulkeith, W. M. Green, and Y. A. Vlasov, "Engineering nonlinearities in nanoscale optical systems: physics and applications in dispersion-engineered silicon nanophotonic wires," Adv. Opt. Photon. **1**, 162–235 (2009).
2. J. Leuthold, C. Koos, and W. Freude, "Nonlinear silicon photonics," Nat. Photonics **4**, 535–544 (2010).
3. J. Meier, W. S. Mohammed, A. Jugessur, L. Qian, M. Mojahedi, and J. S. Aitchison, "Group velocity inversion in AlGaAs nanowires," Opt. Express **15**, 12755–12762 (2007).
4. G. P. Agrawal, *Nonlinear Fiber Optics*, 3rd ed. (Academic, 2001).

5. Q. Lin, O. J. Painter, and G. P. Agrawal, "Nonlinear optical phenomena in silicon waveguides: modeling and applications," Opt. Express **15**, 16604–16644 (2007).
6. A. V. Gorbach and D. V. Skryabin, "Spatial solitons in periodic nanostructures," Phys. Rev. A **79**, 053812 (2009).
7. S. Afshar V. and T. M. Monro, "A full vectorial model for pulse propagation in emerging waveguides with subwavelength structures part I: Kerr nonlinearity," Opt. Express **17**, 2298–2318 (2009).
8. T. X. Tran and F. Biancalana, "An accurate envelope equation for light propagation in photonic nanowires: new nonlinear effects," Opt. Express **17**, 17934–17949 (2009).
9. A. R. Davoyan, I. V. Shadrivov, and Y. S. Kivshar, "Self-focusing and spatial plasmon-polariton solitons," Opt. Express **17**, 21732–21737 (2009).
10. D. V. Skryabin, A. V. Gorbach, and A. Marini, "Surface-induced nonlinearity enhancement of TM modes in planar subwavelength waveguides," J. Opt. Soc. Am. B **28**, 109–114 (2011).
11. A. Marini, R. Hartley, A. V. Gorbach, and D. V. Skryabin, "Surface-induced nonlinearity enhancement in subwavelength rod waveguides," Phys. Rev. A **84**, 063839 (2011).
12. N. C. Panoiu, X. Liu, and J. Osgood, "Self-steepening of ultrashort pulses in silicon photonic nanowires," Opt. Lett. **34**, 947–949 (2009).
13. A. V. Gorbach, X. Zhao, and D. V. Skryabin, "Dispersion of nonlinearity and modulation instability in subwavelength semiconductor waveguides," Opt. Express **19**, 9345–9351 (2011).
14. P. Kinsler and G. H. C. New, "Few-cycle soliton propagation," Phys. Rev. A **69**, 013805 (2004).
15. S. Amiranashvili, U. Bandelow, and N. Akhmediev, "Dispersion of nonlinear group velocity determines shortest envelope solitons," Phys. Rev. A **84**, 043834 (2011).
16. Z. Xu, B. Maes, X. Jiang, J. D. Joannopoulos, L. Torner, and M. Soljačić, "Nonlinear photonic crystals near the supercollimation point," Opt. Lett. **33**, 1762–1764 (2008).
17. Y. Xiang, S. Wen, X. Dai, Z. Tang, W. Su, and D. Fan, "Modulation instability induced by nonlinear dispersion in nonlinear metamaterials," J. Opt. Soc. Am. B **24**, 3058–3063 (2007).
18. J. Gomez-Gardeñes, B. A. Malomed, L. M. Flora, and A. R. Bishop, "Solitons in the Salerno model with competing nonlinearities," Phys. Rev. E **73**, 036608 (2006).
19. W. Ding, O. K. Staines, G. D. Hobbs, A. V. Gorbach, C. de Nobriga, W. J. Wadsworth, J. C. Knight, D. V. Skryabin, M. J. Strain, and M. Sorel, "Modulational instability in a silicon-on-insulator directional coupler: role of the coupling-induced group velocity dispersion," Opt. Lett. **37**, 668–670 (2012).
20. D. V. Skryabin and A. V. Gorbach, "Looking at a soliton through the prism of optical supercontinuum," Rev. Mod. Phys. **82**, 1287–1299 (2010).
21. I.-W. Hsieh, X. Chen, X. Liu, J. I. Dadap, N. C. Panoiu, C.-Y. Chou, F. Xia, W. M. Green, Y. A. Vlasov, and R. M. Osgood, "Supercontinuum generation in silicon photonic wires," Opt. Express **15**, 15242–15249 (2007).
22. A. V. Gorbach, W. Ding, O. K. Staines, C. E. de Nobriga, G. D. Hobbs, W. J. Wadsworth, J. C. Knight, D. V. Skryabin, A. Samarelli, M. Sorel, and R. M. De La Rue, "Spatiotemporal nonlinear optics in arrays of subwavelength waveguides," Phys. Rev. A **82**, 041802 (2010).
23. Q. Lin, J. Zhang, G. Piredda, R. W. Boyd, P. M. Fauchet, and G. P. Agrawal, "Dispersion of silicon nonlinearities in the near infrared region," Appl. Phys. Lett. **91**, 21111 (2007).